Effect of Stub-Position Adjustment of Multi-Mode Resonators in Filtering Antenna

Fajri Darwis, Arief Budi Santiko, Taufiqqurrachman, *Member, IAENG,* Winy Desvasari, R. Priyo Hartono Adji, Dadin Mahmudin, Puput Dani Prasetyo Adi, *Member, IAENG,* Fadil Habibi Danufane, and Ashif Aminulloh Fathnan

Abstract—**This study investigates a filtering antenna design for a Ku-Band satellite terminal, integrating a printed monopole antenna with a multimode resonator filter. The antenna, fed via a 50 Ω transmission line, incorporates resonators into its structure to serve as a filter. By adjusting stub positions, the coupling between resonators and the antenna feed line is optimized. Two models are analyzed and optimized at 12 GHz: the first model places stubs on the right edge, achieving a bandwidth of 2.04 GHz and a realized gain of 6.688 dBi. The second model, with stubs on the left edge, exhibits bandwidth reduction and increased reflection loss at the initial design, resulting in a bandwidth of 2.024 GHz and a realized gain of 6.333 dBi. Measurements confirm bandwidth increases of 40 MHz and 696 MHz for the first and second models, respectively. This research highlights the effectiveness of integrating resonators into antenna designs to enhance bandwidth and performance for mobile satellite terminals at Ku-Band frequencies.**

Index Terms—**coupling, filtenna, resonator, satellite, Ku-Band**

Manuscript received October 20, 2024; revised May 6, 2025

This work was supported by the Organization Research of Electronic and Informatic (OREI), National Research and Innovation Agency (BRIN) through a Rumah Program (RP 2024).

Fajri Darwis is a researcher at Research Center for Telecommunication (PRT), National Research and Innovation Agency (BRIN), Bandung 40135, Indonesia. (corresponding author e-mail: fajr001@brin.go.id).

Arief Budi Santiko is a researcher at Research Center for Telecommunication (PRT), National Research and Innovation Agency (BRIN), Bandung 40135, Indonesia. (e-mail: arie036@brin.go.id).

Taufiqqurrachman is a researcher at Research Center for Telecommunication (PRT), National Research and Innovation Agency (BRIN), Bandung 40135, Indonesia. (e-mail: tauf011@brin.go.id).

Winy Desvasari is a researcher at Research Center for Telecommunication (PRT), National Research and Innovation Agency (BRIN), Bandung 40135, Indonesia. (e-mail: winy001@brin.go.id).

R. Priyo Hartono Adji is a researcher at Research Center for Telecommunication (PRT), National Research and Innovation Agency (BRIN), Bandung 40135, Indonesia. (e-mail: rpri001@brin.go.id).

Dadin Mahmudin is a researcher at Research Center for Telecommunication (PRT), National Research and Innovation Agency (BRIN), Bandung 40135, Indonesia. (e-mail: dadi005@brin.go.id).

Puput Dani Prasetyo Adi is a researcher at Research Center for Telecommunication (PRT), National Research and Innovation Agency (BRIN), Bandung 40135, Indonesia. (e-mail: pupu008@brin.go.id).

Fadil Habibi Danufane is a researcher at Research Center for Telecommunication (PRT), National Research and Innovation Agency (BRIN), Bandung 40135, Indonesia. (e-mail: fadi004@brin.go.id).

Ashif Aminulloh Fathnan is a researcher at the Research Center for Telecommunication (PRT), National Research and Innovation Agency (BRIN), Bandung 40135, Indonesia. (e-mail: ashi001@brin.go.id).

I. Introduction

In recent years, there has been a growing interest in low earth orbit (LEO) satellite constellations due to their low latency, reduced propagation delay, and extensive coverage capabilities [1]. These satellites are particularly valuable in overcoming communication gaps in remote regions. Additionally, the integration of LEO satellite technology with IoT applications and 5G networks [2] has been explored to address the increasing demand for internet access in underserved areas where traditional wired infrastructure is impractical [1], [3]. Operating predominantly in the Ku-Band, these satellites use different frequency bands for uplink and downlink signals. The mobile satellite terminal, crucial for end-user connectivity, necessitates designs that are compact, cost-effective, and efficient [4]. Integration of components, particularly antennas, and filters (termed as filtering antennas or filtennas), contributes significantly to reducing device size and manufacturing costs [4] - [9].

Various configurations of filtennas have been extensively documented in previous studies, including the utilization of the filter synthesis approach and the incorporation of additional or parasitic resonant elements [10]. The filter synthesis design method can yield filtennas with robust filtering performance; however, it necessitates a larger area, making it less suitable for miniaturization. Conversely, compact and low-profile filtenna designs can be achieved by employing resonant elements such as multilayer patches [11], parasitic structures [12], or metasurfaces [13]. Recently, filtennas incorporating multi-mode resonators have demonstrated additional functionalities, such as polarization control [5] and radiation patterning [14]. Despite these advancements, these configurations often exhibit limitations, including impedance mismatches and fixed operating configurations.

This study focuses on designing a filtering antenna for Ku-Band frequencies based on multi-mode resonators consisting of rectangular step impedance stubs. Unlike existing works that often separate antenna and filtering functionalities [6], [15], our approach integrates a single stub into each 50-Ω port to achieve bandpass filtering. Moreover, by exploring two distinct stub positions, we observed new coupling effects that enable adjustable bandwidth. By precisely adjusting the stub position relative to the feed, we can achieve significant variation in bandwidth profiles, offering adaptable bandwidth with minor structural adjustments. These optimized filtering

antenna designs are suitable for most wireless communication applications including mobile satellite terminals in the Ku-Band range, which may address critical needs in satellite communication technology.

II. Antenna Configuration

As shown in Fig. 1, the filtering antenna is fabricated using printed-circuit technology based on a commercially available dielectric substrate Rogers Duroid 5880 with a relative permittivity of 2.2 and a loss tangent of 0.0009. A dielectric substrate thickness of 1.575 mm and a cooper thickness of 0.035 mm was considered for fabrication. As depicted in Fig. 1, the top layer of the filtenna is a printed monopole antenna (PMA) with a rectangular shape that is fed by a 50-Ω transmission line. Here, we utilize a small rectangular patch with a dimension of 2 mm × 11 mm as a stub load to the printed monopole antenna. The gap between the patch and the stub load is 0.5 mm. Furthermore, there are two 50-Ω transmission lines, each with a small rectangular stub on them. A multimode resonator is coupled fed by the 50-Ω transmission lines through these stubs. The ground plane is rectangular on the back side of the patch antenna. Finally, a 50-Ω transmission line is connected by a 50-Ω SMA connector to serve as an input port. Details of the dimensions are shown in Table I and the corresponding design parameters are indicated in Fig. 1.

Table I
Comparison of the Filtennas Parameters.

Parameters	Values (mm)	
	1st Model	2nd Model
W_{sub}, W_{GND}	21	21
L_{sub}	37.7	38.36
L_{GND}	24.2	24.86
W_p	11	11
L_p	7.5	7.5
S_p	0.5	0.5
L_{rp}	2	2
W_{FL}	4.6	4.3
L_{FL}	8	8
S_c	1.45	1
S_l	1.9	2.46
W_{stub}	0.5	0.5
L_{stub}	3.65	3.7
W_{r1}	0.5	0.5
L_{r1}	8.2	8.66
W_{r2}	0.85	0.95
L_{r2}	0.45	0.9
W_{r3}	3.6	4.1
L_{r3}	2.4	2.43

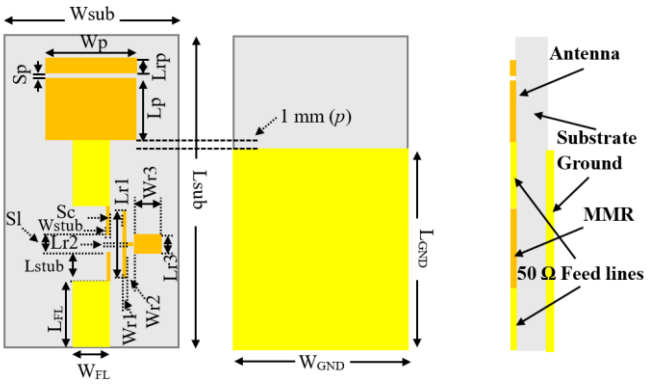

Fig. 1. Proposed filtering antenna.

III. Design and Analysis

A. Radiator Design

The PMA is selected for its capability to support a wide impedance bandwidth, with the lower band-edge frequency estimated using the approximation given in Equation (1) [16].

$$f_L = \frac{7.2}{\{(L + r + p) \times k\}} GHz \quad (1)$$

This formula considers key parameters of the planar monopole antenna, including its height (L), effective radius r, and feed line length p. For this design, a rectangular shape is employed. The constant k is typically approximated as 0.24 and the effective radius r can be estimated using Equation (2) [16]:

$$r = \frac{w}{2\pi} \quad (2)$$

where w is the width of the rectangular monopole. Using dimensions of 7.5 mm in length and 11 mm in width, the estimated lower band-edge frequency is approximately 5 GHz. To further refine the antenna's performance, electromagnetic simulations were conducted, confirming a good return loss at the target frequency and achieving a peak gain of 4.618 dBi at 12 GHz. Performance enhancements were introduced by adding a small rectangular patch (2 mm × 11 mm) adjacent to the antenna, forming a coupling gap as shown in Fig. 2. Parametric analysis of varying gap sizes revealed that a 0.5 mm gap yields the most favorable performance, resulting in the highest gain improvement of

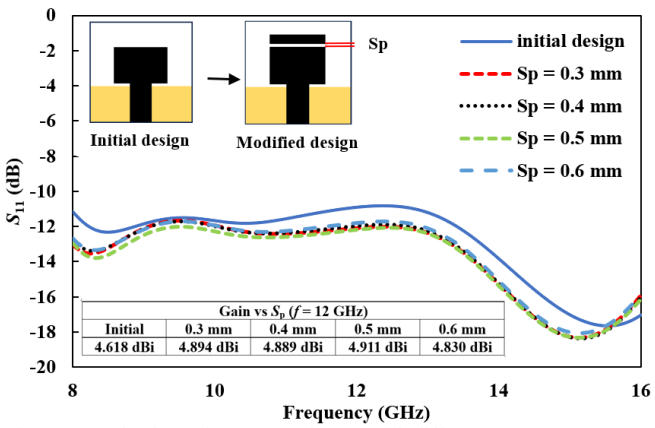

Fig. 2. S_{11} and gain performances of PMA with different S_p.

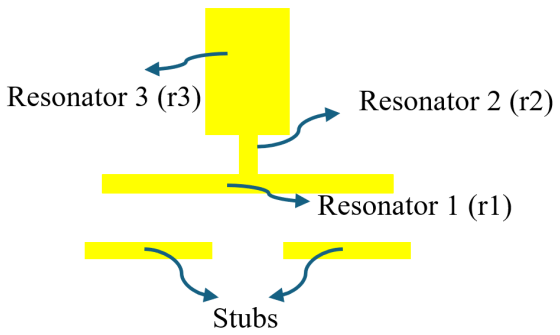

Fig. 3. Configuration of the filter by using a multimode resonator (MMR).

0.293 dBi while maintaining a return loss better than -10 dB. These results serve as the foundation for the next phase, which involves integrating the components to realize the intended filtering functionality.

B. Filter Design and Integration

The filtering circuit is designed to achieve a wide bandwidth by employing a multimode resonator, specifically a step impedance resonator (SIR). This configuration is selected for its advantageous characteristics such as broad impedance bandwidth, favorable transmission and reflection properties, and structural simplicity [15]. As illustrated in Fig. 3, a single-wing bandpass filter is implemented using a rectangular step impedance stub. The design incorporates three impedance resonators: the first, measuring 8.2 mm in length and 0.5 mm in width, is directly coupled to the input and output ports. It is followed by the second resonator (0.45 mm length, 0.85 mm width) and the third resonator (2.4 mm length, 3.6 mm width). The variation in width reflects different impedance levels, with the narrowest width in the first resonator corresponding to the highest impedance. The coupling between the stubs and the ports forms the bandpass response, with the specific gap sizes controlling the coupling strength, as depicted in Fig. 1. The filter's resonance behavior and overall performance are characterized using *S-parameter* analysis.

Next, the filtering circuit is integrated with the radiator, where the bandpass filter (BPF) ports function as the feed line for the planar monopole antenna (PMA), maintaining consistent impedance matching. A 50-Ω transmission line, equipped with a probe feed and connected to the ground plane via a 50-Ω SMA connector, enables seamless integration. Optimization is performed through parametric studies to fine-tune the coupling between the stubs and the filter, as well as between adjacent stubs, with the coupling gaps significantly influencing the bandwidth. As illustrated in Fig. 4, varying the gap S_c while holding S_l constant at 1.9 mm reveals that smaller gaps result in broader bandwidth. An optimal gap of 1.45 mm is selected, yielding a simulated -10 dB bandwidth of approximately 2.04 GHz, spanning from 10.952 GHz to 12.992 GHz.

The investigation reveals that coupling effects extend not only between the filter and stubs but also among the stubs themselves. Fig. 4 illustrates the relationship between stub distance (S_l) and the *S*-parameter, showing that increasing S_l expands the antenna's operating bandwidth. Furthermore, we notice that the SIR's width and length variations significantly impact bandwidth. Figs. 5-7 illustrate S_{11}

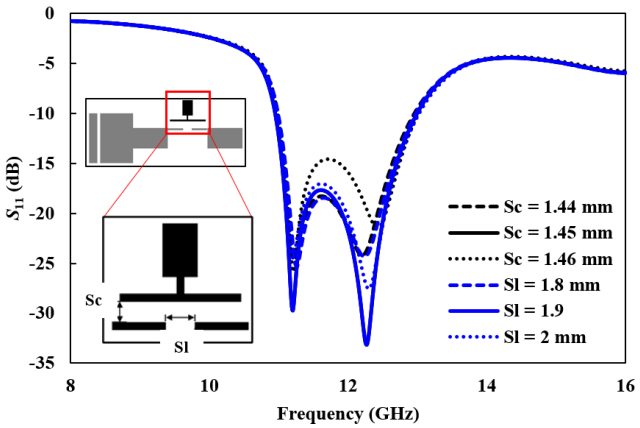

Fig. 4. S_{11} performance of the filtering antenna with different S_c and S_l.

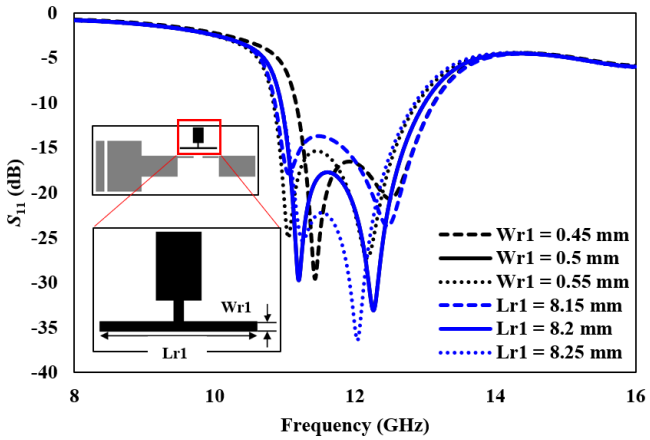

Fig. 5. S_{11} performance of the filtering antenna with different L_{r1} and W_{r1}.

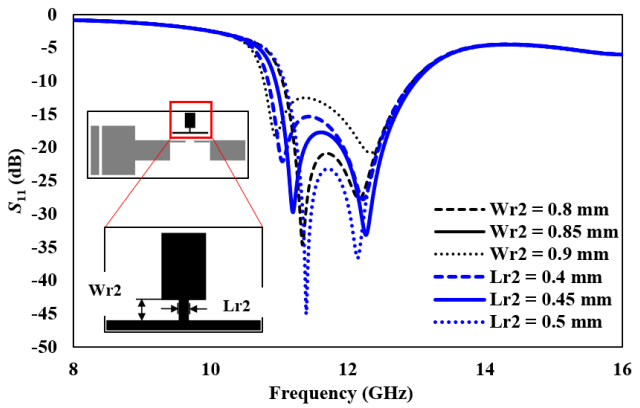

Fig. 6. S_{11} performance of the filtering antenna with different L_{r2} and W_{r2}.

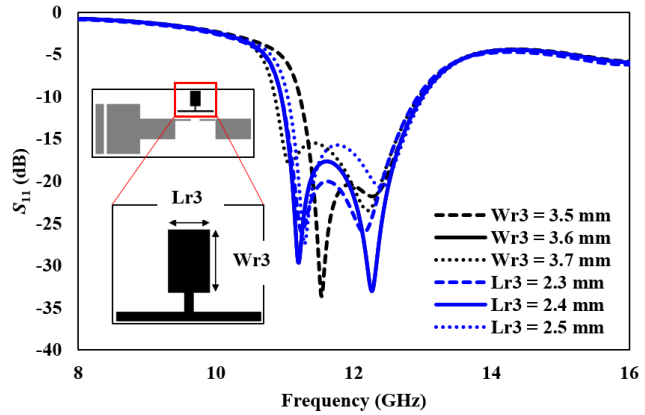

Fig. 7. S_{11} performance of the filtering antenna with different L_{r3} and W_{r3}.

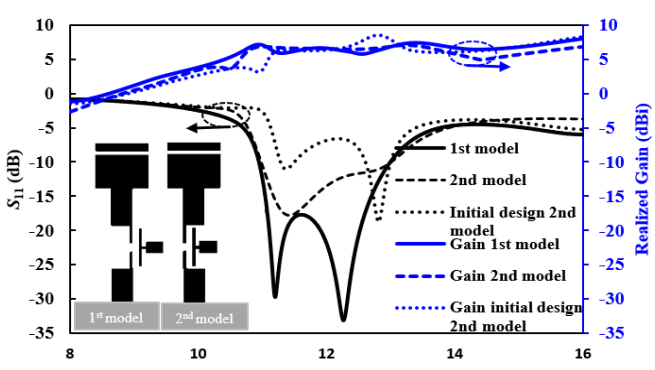

Fig. 8. S_{11} and gain comparison of the filtering antenna with different positions of the filter.

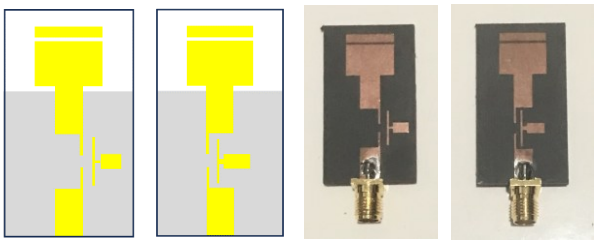

(a) (b) (c) (d)

Fig. 9. The optimized design and fabrication of the filtering antennas, (a) Optimized first model, (b) Optimized second model, (c) Fabricated first model, (d) Fabricated second model.

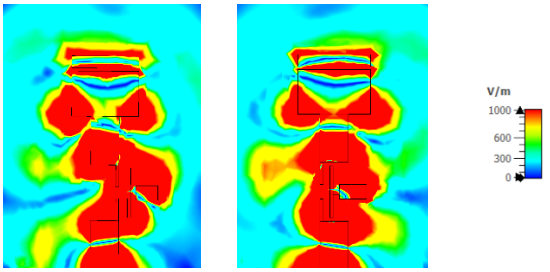

(a) (b)

Fig. 10. The electric field distribution of the filtering antenna (a) First model, (b) Second model.

performance changes with different resonator lengths and widths, affecting both bandwidth and center frequency. Following parametric optimization, stub positions were adjusted in a second model, shifting the MMR to the left edge of the 50 Ω-ports as shown in Fig. 8 to explore the performance of the design with the new coupling between the 50 Ω-ports and the MMR. This adjustment introduced new coupling dynamics between the filter and ports, altering antenna performance. In contrast to the first model where the MMR is on the right edge, the second model positions the filter between ports due to stub placement (Fig. 8). As a result of higher reflection loss, this configuration achieves narrower -10 dB bandwidths, featuring two distinct bands: 216 MHz (from 11.28 GHz to 11.496 GHz) and 392 MHz (from 12.608 GHz to 13 GHz). Nevertheless, the proposed design requires a wide bandwidth. Therefore, parametric optimization will be performed based on the analysis of the first model. As a result, the optimized design of the second model has parameters as shown in Table I.

IV. Results and Discussion

Figs. 9(a) and 9(b) present the optimized integration of two filtering antenna models, which primarily differ in length but share a common width of 21 mm. The second model is slightly longer by 0.66 mm, due to specific optimizations such as stub-to-stub spacing (S_1 = 2.46 mm), stub length (3.7 mm), gap between stubs and resonator (S_c = 1 mm), ground length (24.86 mm), and multimode resonator dimensions (L_{r1} = 8.66 mm, L_{r2} = 0.9 mm, L_{r3} = 2.43 mm, W_{r2} = 0.95 mm, W_{r3} = 4.1 mm).

The two designs exhibit distinct electric field and surface current distributions. Fig. 10 displays the electric field profiles of both filtering antenna models, with the intensity shown in V/m. Notably, a stronger electric field is observed between the 50 Ω feed lines and the multimode resonator (MMR) in the second model, indicating enhanced coupling in this region. Additionally, the bottom edge of the patch in the second model

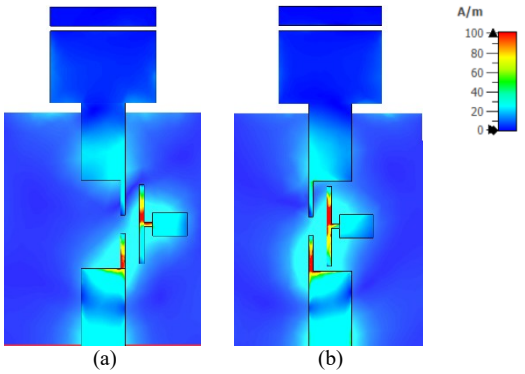

(a) (b)

Fig. 11. The surface current of the filtering antenna (a) First model, (b) Second model.

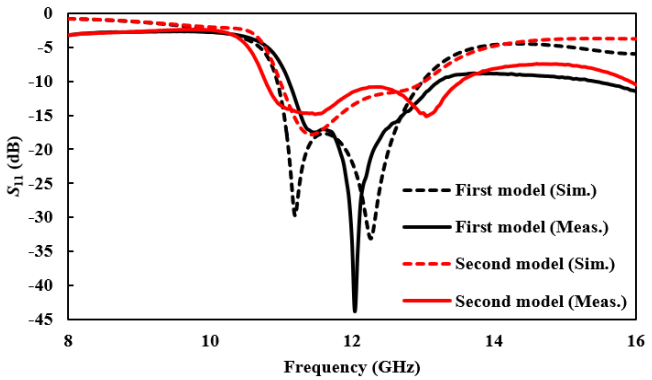

Fig. 12. Simulation and measurement results of the first model and second model of filtering antenna.

shows a higher electric field intensity compared to the first model, which can be attributed to the positioning of the MMR and the feed line width. Fig. 11 shows the surface current distribution for both designs. In both cases, the highest current intensities occur near the MMR. However, the first model exhibits strong current at both the first and second resonators, while the second model shows concentrated intensity only at the first resonator. This variation is influenced by the coupling distance S_c, where the smaller gap in the second model leads to stronger localized coupling.

A. Optimized Filtering Antenna

Fig. 8 compares the initial and optimized designs of the second model's filtering antenna based on the S11 parameter, revealing distinct return loss characteristics. Both versions display two return-to-zero (RZ) points and a central peak, resembling the response of a second-order filter. In the initial design, the reflection coefficient peak remains above –10 dB, suggesting a dual-band filtering response with narrow bandwidth—likely due to unintended coupling effects. However, the design specification calls for a wide bandwidth of approximately 2 GHz.

After optimization, the second model exhibits a single RZ point, with the central peak closely aligned to it, forming a wideband response characteristic of a first-order filter. The center frequencies and –10 dB bandwidths differ slightly between the two models. The first model is centered at 11.972 GHz with a bandwidth of 2.04 GHz (from 10.952 GHz to 12.992 GHz), while the second model centers at 12.004 GHz with a 2.024 GHz bandwidth (from 10.992 GHz to 13.016 GHz). Additionally, the first model

demonstrates a 0.355 dB higher gain than the second, as illustrated in Fig. 8.

B. Measurement

Fabrication and measurement were conducted to validate the filtering antenna designs. Fig. 9 (c) and (d) illustrate the fabricated results for both models. Fig. 12 presents measurement results showing -10 dB impedance bandwidth from S_{11} performance. The first model achieves a bandwidth of 2.08 GHz (11.12 GHz to 13.2 GHz) with a center frequency shifted by 188 MHz from the simulation. In comparison, the second model exhibits a larger bandwidth of 2.72 GHz, with a center frequency shift of 156 MHz from the simulation. The biggest frequency shift occurs at the upper frequencies, around 504 MHz for the second model and 208 MHz for the first model at the upper-frequency range.

The efficiency of the filtenna for both models is presented in Fig. 13. The efficiency of the filtenna in the second model slightly degrades starting at 12 GHz, reaching 95%, while the first model maintains an efficiency of 98%. Fig. 14 shows the measurement setup using a horn antenna connected to the signal generator as a transmitter. On the other side, the filtenna is connected to the spectrum analyzer to capture the signal. Furthermore, Fig. 15 displays the radiation patterns for both models at $\varphi = 90°$ and $\theta = 90°$, showing an identical pattern between simulated and measured data. However, there are slight differences due to substrate dielectric constants and inaccuracies in the fabrication process, which affect the parameter structure, including soldering and the measurement environment.

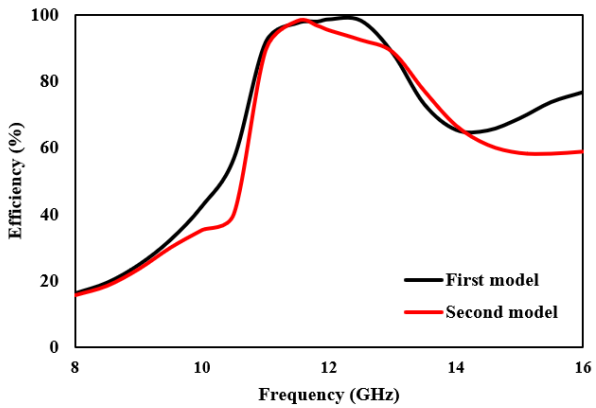

Fig. 13. Efficiency of the first and second model filtennas.

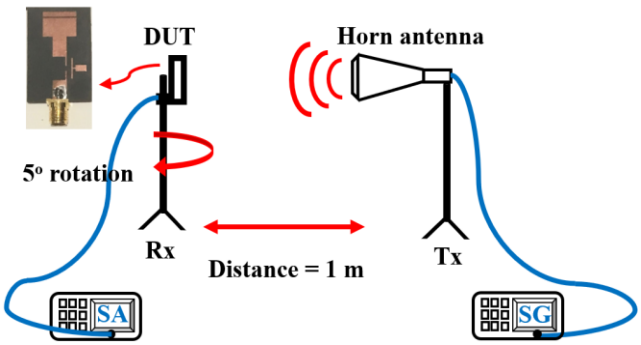

Fig. 14. The experimental setup using horn antenna, signal generator (SG) and spectrum analyzer (SA).

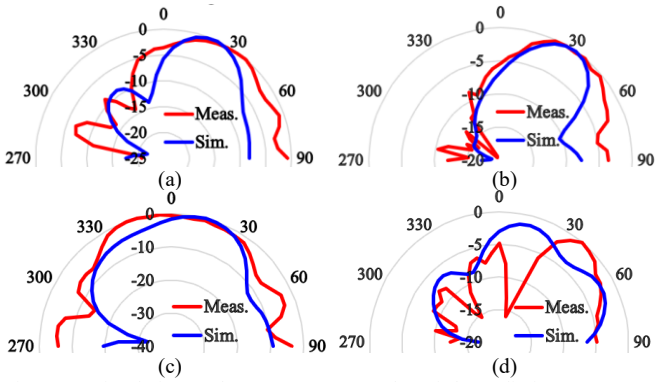

Fig. 15. Simulation and measurement results of the radiation pattern at 12 GHz, (a) First model at plane $\varphi = 90°$, (b) First model at plane $\theta = 90°$, (c) Second model at plane $\varphi = 90°$, (d) Second model at plane $\theta = 90°$.

TABLE II
COMPARISON OF THE PROPOSED FILTENNAS CHARACTERISTICS.

Filtenna		Gain (dB)	Bandwidth (GHz)	Efficiency (%)
First Model	Simulated	6.688	2.04	98
	Measured	3.6	2.08	
Second Model	Simulated	6.333	2.024	95
	Measured	3.2	2.72	

The comparison of the proposed filtenna, including gain, bandwidth, and antenna efficiency, is presented in Table II. The first model has higher values of gain and efficiency, which are 3.6 dB and 98%, respectively. However, the measurement result of the second model shows a wider bandwidth compared to the first model, with a value of 2.72 GHz.

V. CONCLUSION

We introduced a filtering antenna based on a multimode resonator with varying stub resonator positions. This antenna is designed for receiver and signal downlink applications, with potential use in mobile satellite terminals. Our findings indicate that one configuration of stub positioning results in a two distinct band filtering antenna with narrow bandwidth, whereas an alternative configuration yields a broadband filtering antenna with wide bandwidth. Measurement results confirmed significant variations in bandwidth and center frequency shifts. These designs represent promising candidates for mobile satellite terminals as well as other Ku-Band applications.

REFERENCES

[1] L. Jin, L. Wang, X. Jin, J. Zhu, K. Duan, and Z. Li, "Research on the application of LEO satellite in IOT," in *Proc. 2022 IEEE 2nd Int. Conf. Electronic Technology, Communication, and Information*, Changchun, China, 2022, pp. 739–741.

[2] O. T. Eluwole, N. Udoh, M. Ojo, C. Okoro, and A. J. Akinyoade, "From 1G to 5G, what Next?," *IAENG Int. J. Comput. Sci.*, vol. 45, no. 3, pp. 413-434, 2018.

[3] E. P. Wigner, "Theory of traveling-wave optical laser," *Phys. Rev.*, vol. 134, pp. A635–A646, Dec. 1965.

[4] L. Rodrigues, T. Varum, and J. N. Matos, "The application of reconfigurable filtennas in mobile satellite terminals," *IEEE Access*, vol. 8, pp. 77179-77187, 2020.

[5] D. A. Cahyasiwi, F. Y. Zulkifli, and E. T. Rahardjo, "Switchable slant polarization filtering antenna using two inverted resonator structures for 5G application," *IEEE Access*, vol. 8, pp. 224033-224043, 2020.

[6] A. Ramos, T. Varum, and J. N. Matos, "Compact circularly polarized aperture fed patch antenna for LEO satellite constellations," in *Proc.*

2021 IEEE Int. Symp. Antennas and Propagation and USNC-URSI Radio Science Meeting, Singapore, 2021, pp. 379-380.

[7] W. Desvasari et al., "A filtenna design for Ku-band satellite mobile terminal," in *Proc. 2023 Int. Conf. Radar, Antenna, Microwave, Electronics, and Telecommunications*, Bandung, Indonesia, 2023, pp. 269-272.

[8] T. Kanimozhi and S. K. Lalitha, "A compact filtenna for Ku –band application," in *Proc. 2023 IEEE 7th Conf. Information and Communication Technology*, Jabalpur, India, 2023, doi: 10.1109/CICT59886.2023.10455510.

[9] J. W. Wang, J. H. Ou, Y. Z. Niu, W. Yu, H. F. Huang, and X. Y. Zhang, "Dual-circularly polarized aperture-shared filtennas with high isolation for K/Ka-band satellite applications," in *Proc. 2023 IEEE 11th Asia-Pacific Conf. Antennas and Propagation*, Guangzhou, China, 2023, pp. 1-2.

[10] C. X. Mao, Y. Zhang, X. Y. Zhang, P. Xiao, Y. Wang, and S. Gao, "Filtering antennas: design methods and recent developments," *IEEE Microwave Magazine*, vol. 22, no. 11, pp. 52-63, Nov. 2021.X. Y. Zhang, W. Duan, and Y. -M. Pan, "High-gain filtering patch antenna without extra circuit," *IEEE Trans. Antennas and Propagation*, vol. 63, no. 12, pp. 5883-5888, Dec. 2015.

[11] M. Patriotis, F. N. Ayoub, Y. Tawk, J. Costantine, and C. G. Christodoulou, "A compact active Ka-band filtenna for CubeSats," *IEEE Antennas and Wireless Propagation Letters*, vol. 20, no. 11, pp. 2095-2099, Nov. 2021.

[12] Y. M. Pan, P. F. Hu, X. Y. Zhang, and S. Y. Zheng, "A low-profile high-gain and wideband filtering antenna with metasurface," *IEEE Trans. Antennas and Prop.*, vol. 64, no. 5, pp. 2010-2016, May 2016.

[13] K. R. Mahmoud and A. M. Montaser, "Design of compact mm-wave tunable filtenna using capacitor loaded trapezoid slots in ground plane for 5G router applications," *IEEE Access*, vol. 8, pp. 27715-27723, 2020.

[14] S. Ahmed, T. K. Geok, M. Y. Alias, H. Alsariera, A. Abdaziz, and P. J. Soh, "A UWB antenna array integrated with multimode resonator bandpass filter," *Electronics*, vol. 10, no. 5, Art. no. 607, 2021.

[15] K. P. Ray, "Design aspects of printed monopole antennas for ultra-wide band applications", *Int. J. Antennas and Propagation*, vol. 2008, Art. no. 713858, 2008.

Ashif Aminulloh Fathnan received a Doctoral degree from the University of New South Wales (UNSW) Canberra, Australia in February 2021. He is now a researcher at the Research Center for Telecommunication, National Research and Innovation Agency, Indonesia as well as a lecturer at the Department of Electrical Engineering, Telkom University, Indonesia. He received a postdoctoral fellowship award from Japan Society for the Promotion of Science (JSPS) in 2022, LPDP Doctoral Scholarship (2017-2021) from Ministry of Finance, Republic of Indonesia, Young Scientist Award from the International Union of Radio Science (URSI) and Dean's Award for Outstanding PhD Theses from UNSW Australia in 2021. His current research interests include: spectral and spatial dispersion of metasurfaces; tunable metasurfaces for sensing, imaging and communication; and non-linear metasurfaces.